p Orbital Flat Band and Dirac Cone in the Electronic Honeycomb Lattice Article

Thomas S Gardenier, Jette J van den Broeke, Jesper R Moes, Ingmar Swart, Christophe Delerue, Marlou R Slot, C Morais Smith, Daniel Vanmaekelbergh

ACSNANO

www.acsnano.org

ARTICLE

p Orbital Flat Band and Dirac Cone in the Electronic Honeycomb Lattice

Thomas S. Gardenier,[¶] Jette J. van den Broeke,[¶] Jesper R. Moes, Ingmar Swart, Christophe Delerue, Marlou R. Slot, C. Morais Smith, and Daniel Vanmaekelbergh*

Cite This: https://dx.doi.org/10.1021/acsnano.0c05747

Read Online

ACCESS | Metrics & More | Article Recommendations | Supporting Information

ABSTRACT: **Theory anticipates that the in-plane p_x, p_y orbitals in a honeycomb lattice lead to potentially useful quantum electronic phases. So far, p orbital bands were only realized for cold atoms in optical lattices and for light and exciton-polaritons in photonic crystals. For electrons, in-plane p orbital physics is difficult to access since natural electronic honeycomb lattices, such as graphene and silicene, show strong s−p hybridization. Here, we report on electronic honeycomb lattices prepared on a Cu(111) surface in a scanning tunneling microscope that, by design, show (nearly) pure orbital bands, including the p orbital flat band and Dirac cone.**

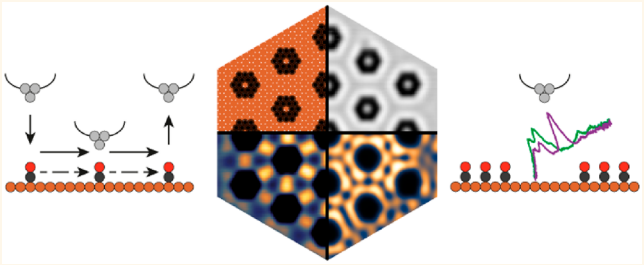

KEYWORDS: *scanning tunneling microscopy (STM), scanning tunneling spectroscopy (STS), electronic lattice, honeycomb, flat band, p orbital, muffin-tin calculations*

The electronic properties of two-dimensional solids, including materials with Dirac bands and topological insulators, are largely determined by the geometry of the atomic lattice and the nature of the interacting orbitals.[1,2] A compelling case is presented by the system of in-plane p_x, p_y orbitals in a honeycomb lattice providing an electronic flat band, due to geometric frustration, and a p-type Dirac cone.[3−5] The in-plane p orbitals in the trigonal honeycomb lattice cannot form conventional bonding−antibonding combinations; their interaction gives rise to complex interference patterns. As a result, the four in-plane p bands consist of a nondispersive flat band, followed by two dispersive bands forming a Dirac cone at higher energy, followed by another flat band. Intrinsic spin−orbit coupling will open a gap at the Dirac point (the quantum spin Hall effect) and detach the flat band from the Dirac cone, making it topological.[6,7] Since the kinetic energy is quenched in the flat band, the dominant energy scale is set by interactions. It has been predicted that this will lead to interesting quantum phases, such as unconventional superconductivity and Wigner crystals.[4,8] The physics of in-plane p orbitals has been studied with ultracold atoms in optical lattices,[8−12] light in photonic systems,[13] and exciton-polaritons in a semiconductor pillar array[14,15] and has been theoretically investigated for real layered materials.[16] However, an experimental realization of an electronic material in which the physics of in-plane p orbitals can emerge by design has not yet been reported.

RESULTS AND DISCUSSION

Natural electronic honeycomb systems show interesting results, but there is considerable hybridization between different types of orbitals.[6] In graphene, the most studied electronic honeycomb lattice, the s orbital and in-plane p_x, p_y orbitals of the carbon atoms hybridize and form sp^2 electronic bands, the lower one being completely filled.[3] This filled band leads to a very strong in-plane bonding between the carbon atoms, but is not electronically active. The remaining p_z orbitals (perpendicular to the graphene plane) form π bonds, resulting in two bands touching at the (K, K′) Dirac points at which the Fermi energy is situated. The linear energy-wave vector dispersion (Dirac cone) around the (K, K′) points is responsible for the electronic properties of graphene.[3] We remark that bilayer graphene twisted at magic angles offers exciting physics whereby interlayer coupling and interacting electrons result in a flat band and unconventional superconductivity.[17,18]

Here, we report solid-state designs for noninteracting electrons in which the physics of in-plane p orbitals fully

Received: July 10, 2020
Accepted: September 29, 2020
Published: September 29, 2020

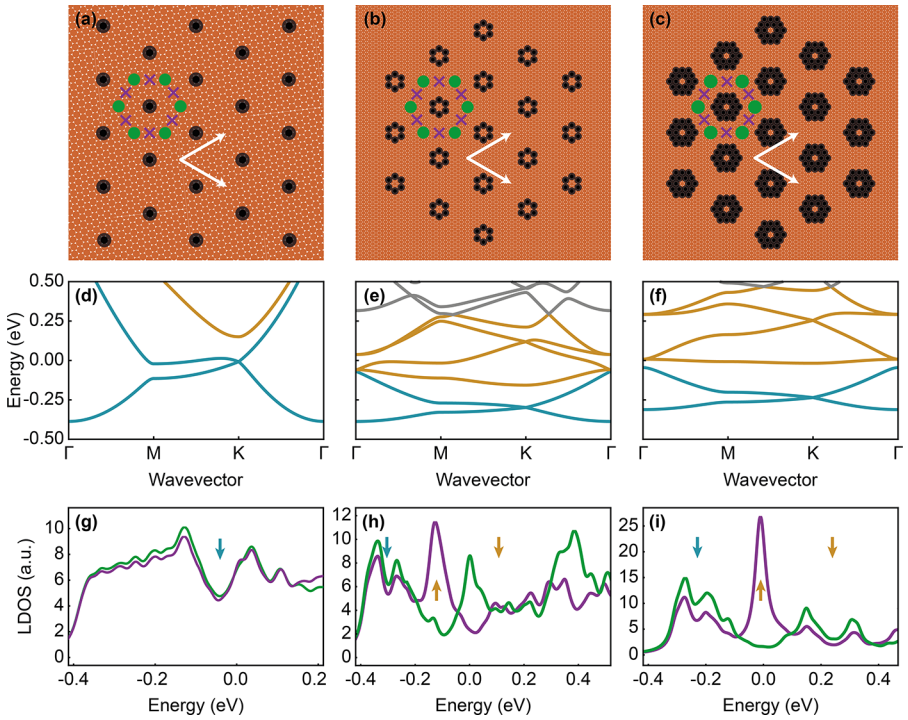

Figure 1. Designs for artificial atoms in a honeycomb lattice, corresponding band structures, and LDOS spectra. (a–c) Schemes of a Cu(111) surface (copper) and the positions of the CO molecules (black) defining the on-site energies of the s and p orbitals and their intersite coupling. The lattice sites are indicated in green; the bridge sites with purple crosses. (a) The lattice reported by Gomes *et al.*,[19] with a honeycomb lattice vector of 1.92 nm. (b) Lattice with single-ringed CO rosettes as scattering islands and a honeycomb lattice vector of 3.58 nm, corresponding to 14 Cu atoms. (c) Lattice with double-ringed CO rosettes as scattering islands; the lattice vector is also 3.58 nm. (d–f) Corresponding band structures calculated by the muffin-tin approximation. The band structures for the designs (b) and (c) reflect (nearly) separated s (blue) and p (orange) orbital bands. (g–i) LDOS for these three designs: green for the on-site positions, purple for the bridge positions between the sites. Blue arrows indicate the s orbital Dirac point; orange arrows indicate the p orbital flat band and the p orbital Dirac point. A broadening of 40 meV is included to account for scattering with the bulk.

emerge. Our work is inspired by the work of Gomes *et al.*, who reported an artificial electronic honeycomb lattice based on the surface-state electrons of a Cu(111) surface.[19] In that work, the confinement of the surface-state electrons in a honeycomb geometry by CO molecules leads to a Dirac cone formed by the first two surface bands at the high symmetry K point. It has been shown afterward that this concept can be extended to create systems with different geometries,[20] fractal structures,[21] nontrivial topology,[22,23] and multiple orbitals by changing the size of the lattice sites.[24] Using this last concept, we design honeycomb lattices consisting of atomic sites with a variable degree of quantum confinement and electronic coupling between them. Muffin-tin calculations show that it is possible to create lattices in which the on-site s orbitals and p orbitals are sufficiently separated such that s–p hybridization can be avoided and Dirac cones and a flat band emerge with nearly pure p orbital character. The band structure is experimentally investigated by measurement of the local density of states and wave function mapping.

The theoretically designed honeycomb lattices are presented in Figure 1, with the original lattice by Gomes *et al.*[19] (Figure 1(a)), and two geometries where the splitting of s and p orbitals is enhanced (*vide infra*) (Figure 1(b, c)). We have calculated the electronic band structure of these lattices by solving the Schrödinger equation with a muffin-tin potential accounting for the rosettes of CO molecules as repulsive scatterers.[25] A broadening of 40 meV was used in the muffin-tin calculations to account for the intrinsic coupling of surface and bulk states in the CO/Cu(111) system. The resulting band structures are presented in Figure 1(d–f). In addition, we fitted the muffin-tin band structure with a tight-binding model based on artificial atomic sites in a honeycomb lattice; each atomic site has one s orbital and two in-plane p orbitals, and we assume s–s, s–p, and p–p hopping between neighboring sites. We obtained excellent agreement between the two band structures for all but the highest bands, as the tight-binding calculation does not take bands of energies higher than the p orbitals into account (see SI Section A and B for more details and fitted parameters). The calculations predict a single Dirac cone (blue color) for the lattice by Gomes *et al.* (Figure 1(d, g)), in agreement with the experimental results reported. For this lattice, our calculations show that the next band (orange color) is strongly dispersive and extends outside the Cu(111) surface state energy window (−0.45 V to +0.5 V). To be able to lower the energy of the p bands, the lattice constant was increased.[19,24] Additionally, to be able to separate the on-site s and p orbitals, we increased the on-site quantum confinement by using single and double CO rosettes as potential barriers. The design presented in Figure 1(b) is based on single CO rosettes.[24] In this case, two dispersive s orbital bands emerge, forming a Dirac cone (blue). The four p orbital bands (orange) contain a (nearly) flat band and two dispersive bands forming a Dirac cone. However, in this design the s and p bands are not separated. We remark here that in the context of real materials, similar-sized lattices of graphene in a graphane matrix have been considered by DFT and tight-binding calculations; in this system, there is strong hybridization between the carbon s and in-plane p_x, p_y orbitals, while the Dirac properties arise from

https://dx.doi.org/10.1021/acsnano.0c05747
ACS Nano XXXX, XXX, XXX–XXX

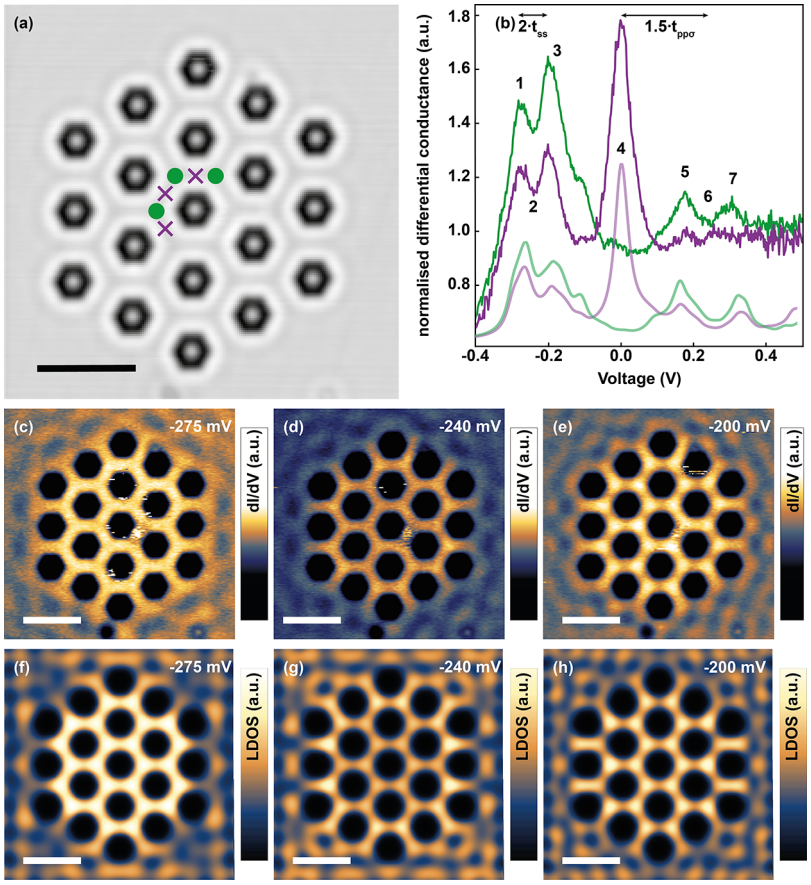

Figure 2. Scanning tunneling spectroscopy and electron probability maps of an artificial honeycomb lattice with separated s and p bands. (a) Scanning tunneling microscopy image (0.5 V, 0.3 nA) of the artificial honeycomb lattice prepared with double-ringed rosettes according to Figure 1(c); a detailed image for a similar lattice is presented in Figure S5. The bright spot in the center of the rosettes is typically found in dI/dV plots at positive bias. Other examples can be found in the SI, Section L. (b) LDOS, *i.e.*, $(dI/dV)_{lattice}/(dI/dV)_{Cu}$, *vs* bias voltage V, measured by scanning tunneling spectroscopy, on top of the artificial atom sites (green) and bridge sites (purple). The LDOS calculated using the muffin-tin approach is replotted in light green and light purple for comparison. The magnitudes of t_{ss} and $t_{pp\sigma}$ are indicated. (c, d, e) Spatially resolved LDOS maps in the energy region of the lowest Dirac cone (points 1−3 in Figure 1(b)) measured at constant height with (f, g, h) the same maps calculated with a muffin-tin potential landscape. The high density of states at the sites reflects s orbital bands. Scale bars are 5 nm.

the coupling of the perpendicular p_z orbitals.[26] In order to prevent this s−p hybridization, the on-site s and p energy levels must be better separated by quantum confinement. This is achieved with the lattice presented in Figure 1(c) (double-ringed CO rosettes as scatterers), showing the p orbital flat band and Dirac cone, well separated in energy from the lower s Dirac cone. The LDOS calculated for designs (b) and (c) (Figure 1(h, i)) display a double peak with a minimum, reflecting the s Dirac cone, followed by a single peak with high LDOS due to the p orbital flat band, followed by a second double peak due to the p orbital Dirac cone. This indicates that our lattices are appropriate electronic quantum simulators for the study of the in-plane p orbital physics.

First, we present an overall electronic characterization of the honeycomb lattice according to the design shown in Figure 1(c). The results on the other lattice (Figure 1(b)) are given in SI Section C. Figure 2(a) shows a scanning tunneling microscope image using a Cu tip. Details are presented in Figure S5, displaying a nearly identical lattice but now imaged with a CO-terminated tip. The LDOS could be probed with scanning tunneling spectroscopy by placing the metallic Cu-coated tip above the center of the artificial sites (green circles in Figures 1(c) and 2(a)) and on bridge sites between the lattice sites (purple crosses); the bias voltage was changed over the entire voltage region of the Cu surface state between V = −0.4 and +0.5 V. The LDOS, *i.e.*, normalized dI/dV *vs* bias voltage,[19] spectra on the on-site and bridge site positions are presented in Figure 2(b); see Figure S6 for details; they should be compared with the theoretical muffin-tin spectra, for convenience replotted from Figure 1(i) in light colors. The first double peak (peaks 1 and 3) corresponds to two s orbital bands forming a Dirac cone; the minimum indicates the Dirac point (point 2). The two maxima correspond to the high LDOS at the M points (see SI Section F); if the overlap integral between neighboring s orbitals is neglected, the distance between these two maxima provide a good estimation for two times the hopping term between the nearest-neighbor s orbitals, *i.e.*, $2t_{ss}$ (see SI Section F). The t_{ss} value that we obtain is 45 meV. From a tight-binding fit, taking the overlap into account, we find 60 meV. The two s orbital bands do not show the typical bonding (lowest s band) and antibonding (higher s band) character. An analytical tight-binding model presented in SI Section B provides a detailed explanation.

Around V = 0 V, a very strong LDOS peak is observed on the bridge sites, while the LDOS on the lattice sites is very low (peak 4). A comparison with the muffin-tin band structure, and

https://dx.doi.org/10.1021/acsnano.0c05747
ACS Nano XXXX, XXX, XXX−XXX

the tight-binding fit to it, reveals that this strong resonance localized between the sites is due to the flat band originating from p orbitals. The high electron probability observed between the lattice sites will be discussed in detail below. Between 0.1 and 0.4 V, we find a second double peak with a minimum. Comparison with our calculations shows that this feature reflects the dispersive p orbital bands; the minimum corresponds to the Dirac point (point 6), and the lower maximum (peak 5) reflects the high LDOS at the M point. The maximum at higher energy (peak 7) corresponds to the third and fourth p orbital bands. If the orbital overlap and residual s−p hybridization are neglected, the energy difference between the flat band maximum and the Dirac point is 1.5 $t_{pp\sigma}$; from this, $t_{pp\sigma}$ is found to be 160 meV. From the muffin-tin calculations combined with a tight-binding fit we find a value of 127 meV (see Table S1).

Figure 2(c, d, e) display energy-resolved LDOS maps in the energy region of the s bands measured over the entire lattice at a constant tip−sample distance, while the panels below (Figure 2(f−h)) show the electron probabilities calculated with the muffin-tin model. There is a good agreement between the observed and calculated LDOS; the large on-site LDOS reflects the on-site *s* orbitals, and the LDOS at the Dirac point is much lower, but does not vanish completely. This reflects a certain broadening of the resonances due to the coupling of the lattice states with surface states outside the lattice and with Cu bulk states. A discussion of the LDOS maps in the s band region from the tight-binding perspective is given in SI Section G.

Maps of the electron probability measured in the energy region of the p bands are presented in Figures 3(a and b); Figures 3(c and d) show the calculated results. The electron probability pattern at the flat-band energy has a very high electron probability between the sites and a very low probability on the sites [Figure 3(a, c) and insets]. In addition, the electron probability (LDOS) map in the region of the p orbital Dirac cone shows detailed patterning [Figure 3(b, d) and inset]; see also SI Section H. The low on-site electron probability on the center of the lattice sites show that these two bands are formed from p orbitals.

The intricately patterned electron probabilities observed in the energy region of the p orbital bands in the honeycomb lattice require further investigation. The interaction of in-plane p orbitals at the sites of a honeycomb lattice can best be described as orbital interference by geometric frustration.[6] We have calculated these interference patterns by using the original tight-binding theory;[4,6] see Figure 4. The results of the muffin-tin calculations combined with a tight-binding parameter fit are presented in Figure S2(c and d). At the flat band energy, different points in the Brillouin zone show distinct interference patterns from the in-plane p orbitals, two of them being presented in Figure 4(a, b). The overall sum of the electron probability patterns over the Brillouin zone at the energy of the flat band is presented in Figure 4(c), showing a strongly enhanced electron probability on the bridge sites, in full agreement with the experimental results. Likewise, as originally proposed in ref 4, Wannier-like eigenstates with the flat band energy can be constructed around each CO rosette of artificial sites resulting in a high electron probability between the lattice sites (also called bridge sites); see Figure 4(d). This spatial electron probability pattern in the flat band agrees with the experimental results and the result of muffin-tin calculations; see Figure 3. In addition, a comparison between Figure 3(b and d) shows that the spatial patterns of the LDOS in the p orbital Dirac region are well reproduced by the muffin-tin calculations.

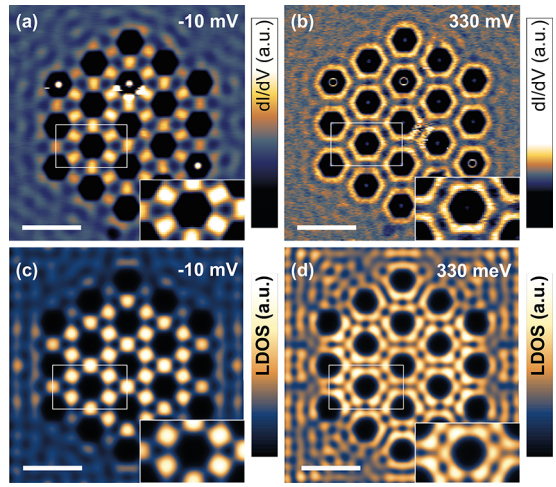

Figure 3. Electron probability (LDOS) maps in the energy region of the p orbital flat band and p orbital Dirac cone obtained by energy-resolved scanning tunneling microscopy at constant height. Spatially resolved LDOS measured at (a) the flat band energy [point 4 in Figure 2(b)] showing patterns of very high electron probability at bridge sites and very low probability on the atomic sites; (b) in the energy region of the p orbital Dirac cone [point 7 in Figure 2(b)]. Several bright spots assigned to mobile hydrogen species are visible in the maps; however, these spots do not perturb the observed pattern. The LDOS calculated using a muffin-tin approach for (c) the flat band showing a pattern of large electron densities between the sites and very low electron density on the sites, to be compared with the experimental result in part (a); (d) energy region of the p orbital Dirac cone, showing a good agreement with the intriguing patterns experimentally observed. More information can be found in the SI. The insets show a magnification. Scale bars are 5 nm.

CONCLUSIONS

Our results show that solid-state electronic honeycomb lattices can be designed in such a way that in-plane p orbital physics fully emerges. The design is purely based on the lattice geometry and the degree of quantum confinement and intersite coupling. These concepts can, therefore, be directly transferred to two-dimensional semiconductors in which the honeycomb geometry is lithographically patterned[27−30] or obtained by nanocrystal assembly.[7,31] Such honeycomb semiconductors can be incorporated in transistor-type devices in which the Fermi level and thus the density of the electron gas can be fully controlled.[30,32] For instance, a partial filling of the flat band can result in electronic Wigner crystals, magnetic phases, and superconductivity.[4,6] Hence, we present a feasible geometric platform for real materials opening the gate to unexpected electronic quantum phases, both in the single-particle regime[7,25,33,34] and in the regime with strong interactions.[35−37]

METHODS

The measurements were obtained in a Scienta Omicron LT-STM. It was operated at a base temperature of 4.5 K and with a pressure in the 10^{-10} mbar range. A clean Cu(111) surface was prepared by multiple sputtering and annealing cycles.[38] CO molecules were deposited on the sample placed in a cooled measurement head by leaking in gas at a pressure of 2×10^{-10} mbar for 3 min. The STM tips were PtIr coated with Cu due to tip preparation. Atomic scale lateral manipulation of

https://dx.doi.org/10.1021/acsnano.0c05747
ACS Nano XXXX, XXX, XXX−XXX

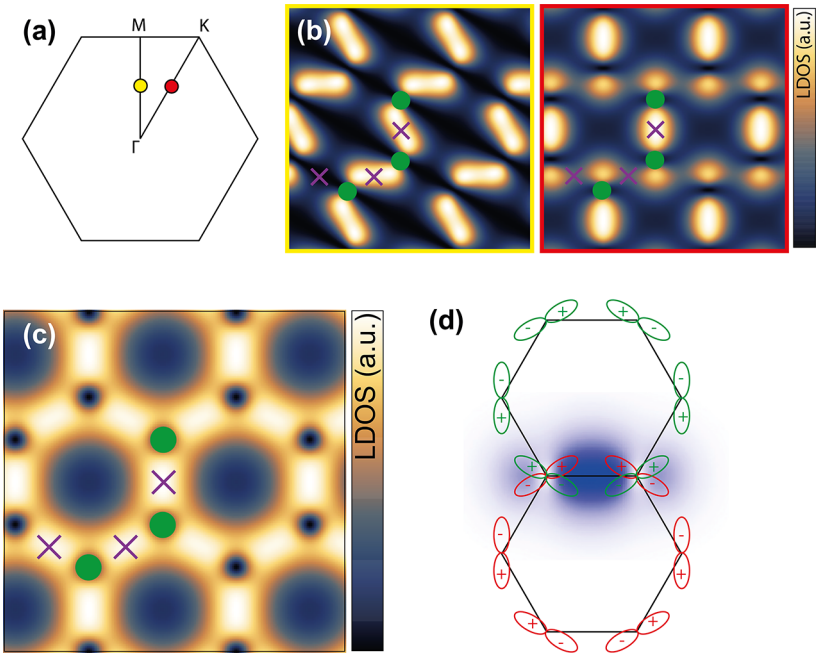

Figure 4. Tight-binding calculation of the interference patterns of the in-plane p_x, p_y orbitals in the honeycomb geometry and the resulting electron probabilities in the p-type flat band. (a) Scheme of the Brillouin zone with Γ, M, and K points indicated. The yellow (red) circles denote the positions in the zone used in panel (b). (b) Two spatial patterns due to interference of the p_x, p_y orbitals in the honeycomb geometry at the flat band energy (−0.01 V) at the two points in the Brillouin zone indicated in panel (a). Artificial atom sites (green) and bridge sites (purple) are indicated. (c) Overall electron probability at the flat band energy obtained from the interference patterns (see panel (b)) and summed over the entire Brillouin zone. Strong electron probabilities are observed on bridge sites (purple crosses) as in the experimental maps. (d) Representation of the electron probability map at the flat band energy by construction of Wannier-like eigenstates from p orbitals organized around a hexagon. The dark blue color indicates high electron probability. See also Figure S9(c).

the CO molecules was performed to build the honeycomb lattices using previously obtained parameters of 40 nA and 10 mV.[19,39,40] Unless mentioned otherwise, all STM topography images were acquired at a constant current of 1 nA and 500 mV. Wave function mapping and differential conductance spectroscopy were performed using constant-height mode with a lock-in amplifier providing a 273 Hz bias modulation with an amplitude between 5 and 20 mV rms. Experimental data were analyzed with the SPM analysis software Gwyddion 2.49 and/or Python 3.7.

The design of the CO rosettes was determined by previously acquired knowledge about CO manipulation[19] and muffin-tin band structure calculations. The double-ringed rosette consists of 18 CO molecules arranged in two rings placed around a central (empty) Cu lattice site as shown in Figure 1(c). This central site was left clear for ease of building. The rosettes were placed at a 3.58 nm spacing (14 Cu atomic sites) along close-packed Cu atomic rows.

All band structures and theoretical LDOS maps shown Figure 1−3 of the main text were calculated using the muffin-tin model. The surface state of Cu(111) is modeled as a two-dimensional electron gas with an effective electron mass of 0.42 times the free electron mass, at a constant potential. The CO molecules are portrayed as discs with a diameter of 0.6 nm and a repulsive potential of 0.9 eV. These parameters were used previously to successfully describe the CO on a copper system.[20] When CO molecules were placed close together and the radii overlapped, the potential of that area was added together and increased to 1.8 eV. The one-electron Schrödinger equation was solved numerically for this system to determine the band structure (periodic case) and LDOS maps (finite size). For the LDOS maps, Neumann boundary conditions were applied. In order to obtain the maps shown, a broadening of 0.04 eV was included.

ASSOCIATED CONTENT

Supporting Information

The Supporting Information is available free of charge at https://pubs.acs.org/doi/10.1021/acsnano.0c05747.

Additional information (PDF)

AUTHOR INFORMATION

Corresponding Author

Daniel Vanmaekelbergh − *Debye Institute for Nanomaterials Science, Utrecht University, 3508 TA Utrecht, The Netherlands;* orcid.org/0000-0002-3535-8366; Email: D.Vanmaekelbergh@uu.nl

Authors

Thomas S. Gardenier − *Debye Institute for Nanomaterials Science, Utrecht University, 3508 TA Utrecht, The Netherlands;* orcid.org/0000-0002-5100-7996

Jette J. van den Broeke − *Institute for Theoretical Physics, Utrecht University, 3508 TB Utrecht, The Netherlands;* orcid.org/0000-0001-5935-5074

Jesper R. Moes − *Debye Institute for Nanomaterials Science, Utrecht University, 3508 TA Utrecht, The Netherlands*

Ingmar Swart − *Debye Institute for Nanomaterials Science, Utrecht University, 3508 TA Utrecht, The Netherlands;* orcid.org/0000-0003-3201-7301

Christophe Delerue − *Université de Lille, F-59000 Lille, France;* orcid.org/0000-0002-0427-3001

Marlou R. Slot − *Debye Institute for Nanomaterials Science, Utrecht University, 3508 TA Utrecht, The Netherlands*

C. Morais Smith − *Institute for Theoretical Physics, Utrecht University, 3508 TB Utrecht, The Netherlands*

https://dx.doi.org/10.1021/acsnano.0c05747
ACS Nano XXXX, XXX, XXX−XXX

Complete contact information is available at: https://pubs.acs.org/10.1021/acsnano.0c05747

Author Contributions

[¶]T. S. Gardenier and J. J. van den Broeke contributed equally.

Notes

The authors declare no competing financial interest.

ACKNOWLEDGMENTS

Financial support from the Foundation for Fundamental Research on Matter (FOM, grants 16PR3245 and DDC13), which is part of The Netherlands Organization for Scientific Research (NWO), as well as the European Research Council (Horizon 2020 "FIRSTSTEP", 692691), is gratefully acknowledged.

REFERENCES

(1) Keimer, B.; Moore, J. E. The Physics of Quantum Materials. *Nat. Phys.* **2007**, *13*, 1045−1055.
(2) Bradlyn, B.; Elcoro, L.; Cano, J.; Vergniory, M. G.; Wang, Z.; Felser, C.; Aroyo, M. I.; Bernevig, B. A. Topological Quantum Chemistry. *Nature* **2017**, *547*, 298−305.
(3) Castro Neto, A. H.; Guinea, F.; Peres, N. M. R.; Novoselov, K. S.; Geim, A. K. The Electronic Properties of Graphene. *Rev. Mod. Phys.* **2009**, *81*, 109−162.
(4) Wu, C.; Bergman, D.; Balents, L.; Das Sarma, S. Flat Bands and Wigner Crystallization in the Honeycomb Optical Lattice. *Phys. Rev. Lett.* **2007**, *99*, 070401.
(5) Qiu, W.-X; Ma, L.; Lü, J.-T.; Gao, J.-H. Making Artificial $p_{x,y}$-Orbital Honeycomb Electron Lattice on Metal Surface. **2019**, 1901.01008. *arXiv*. https://arxiv.org/abs/1901.01008 (accessed July 10, 2020).
(6) Reis, F.; Li, G.; Dudy, L.; Bauernfeind, M.; Glass, S.; Hanke, W.; Thomale, R.; Schäfer, J.; Claessen, R. Bismuthene on a SiC Substrate: A Candidate for a High-Temperature Quantum Spin Hall Material. *Science* **2017**, *357*, 287−290.
(7) Kalesaki, E.; Delerue, C.; Morais Smith, C.; Beugeling, W.; Allan, G.; Vanmaekelbergh, D. Dirac Cones, Topological Edge States, and Nontrivial Flat Bands in Two-Dimensional Semiconductors with a Honeycomb Nanogeometry. *Phys. Rev. X* **2014**, *4*, 011010.
(8) Wu, C.; Das Sarma, S. Px, y-Orbital Counterpart of Graphene: Cold Atoms in the Honeycomb Lattice. *Phys. Rev. B: Condens. Matter Mater. Phys.* **2008**, *77*, 235107.
(9) Wu, C.; Liu, W. V.; Moore, J.; Das Sarma, S. Quantum Stripe Ordering in Optical Lattices. *Phys. Rev. Lett.* **2006**, *97*, 190406.
(10) Muller, T.; Folling, S.; Widera, A.; Bloch, I. State Preparation and Dynamics of Ultracold Atoms in Higher Lattice Orbitals. *Phys. Rev. Lett.* **2007**, *99*, 200405.
(11) Olschlager, M.; Kock, T.; Wirth, G.; Ewerbeck, A.; Morais Smith, C.; Hemmerich, A. Interaction-Induced Chiral $p(x) \pm ip(y)$ Superfluid Order of Bosons in an Optical Lattice. *New J. Phys.* **2013**, *15*, 083041.
(12) Wirth, G.; Olschlager, M.; Hemmerich, A. Evidence for Orbital Superfluidity in the *P*-band of a Bipartite Optical Square Lattice. *Nat. Phys.* **2011**, *7*, 147−153.
(13) Milicevic, M.; Ozawa, T.; Montambaux, G.; Carusotto, I.; Galopin, E.; Lemaitre, A.; Le Gratiet, L.; Sagnes, I.; Bloch, J.; Amo, A. Orbital Edge States in a Photonic Honeycomb Lattice. *Phys. Rev. Lett.* **2017**, *118*, 107403.
(14) Jacqmin, T.; Carusotto, I.; Sagnes, I.; Abbarchi, M.; Solnyshkov, D. D.; Malpuech, G.; Galopin, E.; Lemaitre, A.; Bloch, J.; Amo, A. Direct Observation of Dirac Cones and a Flatband in a Honeycomb Lattice for Polaritons. *Phys. Rev. Lett.* **2014**, *112*, 116402.
(15) Klembt, S.; Harder, T. H.; Egorov, O. A.; Winkler, K.; Ge, R.; Bandres, M. A.; Emmerling, M.; Worschech, L.; Liew, T. C. H.; Segev, M.; Schneider, C. Exciton-Polariton Topological Insulator. *Nature* **2018**, *562*, 552−556.
(16) Zeng, J.; Lu, M.; Liu, H.; Jiang, H.; Xie, X. C. Degenerate p Orbitals Flat Band Model and Realization in Two Dimensional Materials. **2020**, 2003.03034. *arXiv*. https://arxiv.org/abs/2003.03034 (accessed August 7, 2020).
(17) Cao, Y.; Fatemi, V.; Fang, S.; Watanabe, K.; Taniguchi, T.; Kaxiras, E.; Jarillo-Herrero, P. Unconventional Superconductivity in Magic-Angle Graphene Superlattices. *Nature* **2018**, *556*, 43−50.
(18) Cao, Y.; Fatemi, V.; Demir, A.; Fang, S.; Tomarken, S. L.; Luo, J. Y.; Sanchez-Yamagishi, J. D.; Watanabe, K.; Taniguchi, T.; Kaxiras, E.; Ashoori, R. C.; Jarillo-Herrero, P. Correlated Insulator Behaviour at Half-Filling in Magic-Angle Graphene Superlattices. *Nature* **2018**, *556*, 80−84.
(19) Gomes, K. K.; Mar, W.; Ko, W.; Guinea, F.; Manoharan, H. C. Designer Dirac Fermions and Topological Phases in Molecular Graphene. *Nature* **2012**, *483*, 306−310.
(20) Slot, M. R.; Gardenier, T. S.; Jacobse, P. H.; van Miert, G. C. P.; Kempkes, S. N.; Zevenhuizen, S. J. M.; Morais Smith, C.; Vanmaekelbergh, D.; Swart, I. Experimental Realization and Characterization of an Electronic Lieb Lattice. *Nat. Phys.* **2017**, *13*, 672−676.
(21) Kempkes, S. N.; Slot, M. R.; Freeney, S. E.; Zevenhuizen, S. J. M.; Vanmaekelbergh, D.; Swart, I.; Morais Smith, C. Design and Characterization of Electrons in a Fractal Geometry. *Nat. Phys.* **2019**, *15*, 127−131.
(22) Kempkes, S. N.; Slot, M. R.; van den Broeke, J. J.; Capiod, P.; Benalcazar, W. A.; Vanmaekelbergh, D.; Bercioux, D.; Swart, I.; Morais Smith, C. Robust Zero-Energy Modes in an Electronic Higher-Order Topological Insulator. *Nat. Mater.* **2019**, *18*, 1292−1297.
(23) Freeney, S. E.; van den Broeke, J. J.; Harsveld van der Veen, A. J. J.; Swart, I.; Morais Smith, C. Edge-Dependent Topology in Kekule Lattices. *Phys. Rev. Lett.* **2020**, *124*, 236404.
(24) Slot, M. R.; Kemkes, S. N.; Knol, E. J.; van Weerdenburg, W. M. J.; van den Broeke, J. J.; Wegner, D.; Vanmaekelbergh, D.; Khajetoorians, A. A.; Morais Smith, C.; Swart, I. *p*-Band Engineering in Artificial Electronic Lattices. *Phys. Rev. X* **2019**, *9*, 011009.
(25) Park, C.-H.; Louie, S. G. Making Massless Dirac Fermions from a Patterned Two-Dimensional Electron Gas. *Nano Lett.* **2009**, *9*, 1793−1797.
(26) Singh, A. K.; Penev, E. S.; Yakobson, B. I. Vacancy Clusters in Graphane as Quantum Dots. *ACS Nano* **2010**, *4* (6), 3510−3514.
(27) Post, L. C.; Xu, T.; Vergel, N. A. F.; Tadjine, A.; Lambert, Y.; Vaurette, F.; Yarekha, D.; Desplanque, L.; Stiévenard, D.; Wallart, X.; Grandidier, B.; Delerue, C.; Vanmaekelbergh, D. Triangular Nanoperforation and Band Engineering of InGaAs Quantum Wells: A Lithographic Route toward Dirac Cones in III-V Semiconductors. *Nanotechnology* **2019**, *30*, 155301.
(28) Gibertini, M.; Singha, A.; Pellegrini, V.; Polini, M. Engineering Artificial Graphene in a Two-Dimensional Electron Gas. *Phys. Rev. B: Condens. Matter Mater. Phys.* **2009**, *79*, 241406.
(29) Singha, A.; Gibertini, M.; Karmakar, B.; Yuan, S.; Polini, M.; Vignale, G.; Katsnelson, M. I.; Pinczuk, A.; Pfeiffer, L. N.; West, K. W.; Pellegrini, V. Two-Dimensional Mott-Hubbard Electrons in an Artificial Honeycomb Lattice. *Science* **2011**, *332*, 1176−1179.
(30) Wang, S.; Scarabelli, D.; Du, L.; Kuznetsova, Y. Y.; Pfeiffer, L. N.; West, K. W.; Gardner, G. C.; Manfra, M. J.; Pellegrini, V.; Wind, S. J.; Pinczuk, A. Observation of Dirac Bands in Artificial Graphene in Small-Period Nanopatterned GaAs Quantum Wells. *Nat. Nanotechnol.* **2018**, *13*, 29.
(31) Boneschanscher, M. P.; Evers, W. H.; Geuchies, J. J.; Altantzis, T.; Goris, B.; Rabouw, F. T.; van Rossum, S. A. P.; van der Zant, H. S. J.; Siebbeles, L. D. A.; Van Tendeloo, G.; Swart, I.; Hilhorst, J.; Petukhov, A. V.; Bals, S.; Vanmaekelbergh, D. Long-Range Orientation and Atomic Attachment of Nanocrystals in 2D Honeycomb Superlattices. *Science* **2014**, *344*, 1377−1380.
(32) Jazi, M. A.; Janssen, V. A. E. C.; Evers, W. H.; Tadjine, A.; Delerue, C.; Siebbeles, L. D. A.; van der Zant, H. S. J.; Houtepen, A. J.; Vanmaekelbergh, D. Transport Properties of a Two-Dimensional

PbSe Square Superstructure in an Electrolyte-Gated Transistor. *Nano Lett.* **2017**, *17*, 5238−5243.
(33) Kane, C. L.; Mele, E. J. Quantum Spin Hall Effect in Graphene. *Phys. Rev. Lett.* **2005**, *95*, 226801.
(34) Beugeling, W.; Kalesaki, E.; Delerue, C.; Niquet, Y.-M.; Vanmaekelbergh, D.; Morais Smith, C. Topological States in Multi-Orbital HgTe Honeycomb Lattices. *Nat. Commun.* **2015**, *6*, 6316.
(35) Rachel, S. Interacting Topological Insulators: A Review. *Rep. Prog. Phys.* **2018**, *81*, 116501.
(36) Laubach, M.; Reuther, J.; Thomale, R.; Rachel, S. Rashba Spin-Orbit Coupling in the Kane-Mele-Hubbard Model. *Phys. Rev. B: Condens. Matter Mater. Phys.* **2014**, *90*, 165136.
(37) Bermudez, A.; Goldman, N.; Kubasiak, A.; Lewenstein, M.; Martin-Delgado, M. A. Topological Phase Transitions in the Non-Abelian Honeycomb Lattice. *New J. Phys.* **2010**, *12*, 033041.
(38) Musket, R. G.; McLean, W.; Colmenares, C. A.; Makowiecki, D. M.; Siekhaus, W. J. Preparation of Atomically Clean Surfaces of Selected Elements: A Review. *Appl. Surf. Sci. (1977-1985)* **1982**, *10*, 143−207.
(39) Celotta, R. J.; Balakirsky, S. B.; Fein, A. P.; Hess, F. M.; Rutter, G. M.; Stroscio, J. A. Invited Article: Autonomous Assembly of Atomically Perfect Nanostructures Using a Scanning Tunneling Microscope. *Rev. Sci. Instrum.* **2014**, *85*, 121301.
(40) Bartels, L.; Meyer, G.; Rieder, K.-H. Basic Steps Involved in the Lateral Manipulation of Single CO Molecules and Rows of CO Molecules. *Chem. Phys. Lett.* **1997**, *273*, 371−375.

https://dx.doi.org/10.1021/acsnano.0c05747
ACS Nano XXXX, XXX, XXX−XXX